

**NASA Technical Memorandum 104644**

# **Design, Development, and Test-Flight of the Rayleigh Scattering Attitude Sensor**

**E. Hilsenrath, E. C. Anderson, D. Flittner, D. Heath, S. Janz, J. Medeiros,  
J. Cerullo, C. Thorpe, and T. Riley**

**September 1997**



# **Design, Development, and Test-Flight of the Rayleigh Scattering Attitude Sensor**

**E. Hilsenrath  
C. Thorpe  
T. Riley**  
*Goddard Space Flight Center  
Greenbelt, MD*

**E. C. Anderson**  
*New Millennium Astronautics  
Charlottesville, VA*

**D. Flittner**  
*University of Arizona  
Tucson, AZ*

**D. Heath**  
*Research and Support Industries  
Boulder, CO*

**S. Janz  
J. Medeiros  
J. Cerullo**  
*IDEA  
Beltsville, MD*



National Aeronautics and  
Space Administration

**Goddard Space Flight Center**  
Greenbelt, Maryland  
**1997**

### ACKNOWLEDGMENTS

The personnel involved in the development of RSAS were supported under NASA contracts NAS5-31729, NAS5-31755, and NASA cooperative agreement NCC5-92. The authors wish to thank Mr. Thomas J. Kelly of Hughes STX for his assistance in obtaining the PATH product, as well as his helpful suggestions. The efforts of the entire SSBUV team should also be acknowledged in providing excellent support, without which the implementation of RSAS would not have been possible. Finally, the authors wish to thank Mr. Patrick E. Frith, for his editing contributions and overall assistance in the publishing of this manuscript.

### NOTE

The list below shows all the authors who contributed to this document. Their current affiliation is shown and, in some cases, their affiliation at the time they contributed to this document.

Affiliation at the time of their contribution/Present affiliation

E. Hilsenrath, Goddard Space Flight Center  
E. C. Anderson, New Millennium Astronautics/ Analytical Graphics  
D. Flittner, University of Arizona  
D. Heath, Research and Support Industries  
S. Janz, IDEA/University of Maryland  
J. Medeiros, IDEA/Allied Signal  
J. Cerullo, IDEA/OMITRON  
C. Thorpe, Goddard Space Flight Center  
T. Riley, Goddard Space Flight Center

Available from:

NASA Center for AeroSpace Information  
800 Elkridge Landing Road  
Linthicum Heights, MD 21090-2934  
Price Code: A17

National Technical Information Service  
5285 Port Royal Road  
Springfield, VA 22161  
Price Code: A10

# TABLE OF CONTENTS

LIST OF FIGURES .....	v
LIST OF TABLES .....	v
GLOSSARY OF TERMS .....	vii
ABSTRACT .....	ix
1. INTRODUCTION .....	1
2. DESIGN .....	1
2.1 Requirements Overview .....	1
2.1.1 RSAS Attitude Determination .....	1
2.1.2 Physical Description .....	2
2.2 System Overview .....	3
2.3 Radiometric Characterization .....	3
2.4 Hardware Design .....	4
2.4.1 Mechanical Description .....	4
2.4.2 Electrical Description .....	4
2.5 Software Design .....	6
2.5.1 RSAS Component Drivers .....	6
2.5.2 Ground Support Equipment Software .....	6
2.5.3 RSAS Data Processing .....	7
2.6 Testing and Calibration .....	7
2.6.1 Optical Calibration .....	7
2.6.2 Structural/Mechanical Analysis and Testing .....	8
2.6.3 Thermal Environment Analysis .....	8
3. PERFORMANCE.....	8
3.1 STS-72 Payload Configuration .....	9
3.2 Analysis Methodology .....	9
3.3 Results .....	10
4. SUMMARY .....	11
REFERENCES .....	11

## LIST OF FIGURES

Figure 1.	Limb viewing geometry .....	2
Figure 2.	Optics module .....	2
Figure 3.	RSAS system diagram .....	3
Figure 4.	RSAS mounted in SSBUV GAS canister .....	5
Figure 5.	RSAS electrical block diagram .....	6
Figure 6.	Variation in pre-flight to post-flight filter transmittance .....	8
Figure 7.	STS-72 payload orientation .....	9
Figure 8.	Model radiance and radiance ratio under various lighting conditions .....	10
Figure 9.	Normalized radiance vs. altitude .....	10
Figure 10.	Elevation angle measured by RSAS and PATH .....	11
Figure 11.	Differences in elevation angle as measured by RSAS, PATH, and SSBUV Sun sensor .....	11

## LIST OF TABLES

Table 1.	Limb Radiance for Minimum and Maximum BSDF at Three Altitudes .....	4
Table 2.	Optical Characteristics .....	4
Table 3.	Expected Stress Levels .....	8

## GLOSSARY OF TERMS

A/D	- analog to digital
APACS	- Atmospheric Pollution, Aerosol and Chemistry Satellite
BSDF	- bi-directional scattering distribution function
EMI	- electromagnetic interference
FIFO	- first-in, first-out
FPGA	- field programmable gate array
FWHM	- full width at half maximum
GAS	- Get Away Special
GSFC	- Goddard Space Flight Center
GSE	- ground support equipment
FOV	- field of view
IR	- infrared
LORE	- Limb Ozone Retrieval Experiment
PATH	- post-flight attitude and trajectory history
PCB	- printed circuit board
RSAS	- Rayleigh Scattering Attitude Sensor
S/N	- signal-to-noise
S/P	- signal per pixel
SOLSE	- Shuttle Ozone Limb Sounding Experiment
SSBUV	- Shuttle Solar Backscatter Ultraviolet
SZA	- solar zenith angle
TOMS	- Total Ozone Mapping Spectrometer
UV	- ultraviolet

## ABSTRACT

The Rayleigh Scattering Attitude Sensor (RSAS), a proof-of-concept device, was designed, developed, and tested at the NASA Goddard Space Flight Center. The prototype instrument was flown aboard the Space Shuttle Endeavor (STS-72) in January 1996. RSAS uses a 512-element linear photodiode array and an interference filter to measure incident solar radiation that is Rayleigh-scattered from the Earth's limb at a wavelength of 355 nm. System requirements and a system overview are presented. Design and development of mechanical, electrical, and optical subsystems of RSAS are also documented, including the software interface structure and ground support equipment (GSE). Pre-flight and post-flight testing procedures, calibration, and optical characterization results are discussed. Limb scattering radiances observed by RSAS during the test-flight show good agreement with predictions by the GSFC ultraviolet radiative transfer model. The attitude determination algorithm applied to the limb scattered signal is presented. The attitude measured by RSAS is shown to be in excellent agreement with concurrent Shuttle pointing data ( $\pm 0.05^\circ$ ). These data indicate that RSAS-type instruments could yield significantly better performance ( $\sim 0.01^\circ$  resolution) than state-of-the-art horizon sensors ( $\sim 0.1^\circ$  resolution), at a considerably lower cost.

# 1.0 INTRODUCTION

Recent theoretical and technological advancements have motivated the design, development, and test-flight of the Rayleigh Scattering Attitude Sensor (RSAS), which uses a linear photodiode array and an interference filter to measure incident solar radiation that is Rayleigh-scattered from the Earth's limb at a wavelength of 355 nm. Currently, the Goddard Space Flight Center (GSFC) ultraviolet radiative transfer code accurately models atmospheric ultraviolet (UV) scattering at this wavelength. This algorithm has been employed for over two decades in the analysis of satellite ozone data from atmospheric UV remote sensors such as the Total Ozone Mapping Spectrometer (TOMS) and the Shuttle Solar Backscatter Ultraviolet (SSBUV)<sup>a</sup> instrument. More recently the model has been used to compute radiance in the Earth's limb from Rayleigh scattered sunlight. By comparing measurements made by RSAS with this computational model of UV radiance versus altitude, the spacecraft attitude can be accurately determined.

The development of RSAS received funding through the GSFC Director's Discretionary Fund. Instrument development (including its optical, electronic, mechanical, and support subsystems) progressed through the phase-A conceptual design, critical design, fabrication, testing, calibration, and payload integration stages in only 10 months. During its initial test flight aboard STS-72 (launched January 11, 1996), RSAS shared the SSBUV instrument's mechanical platforms and used its existing power and data systems.

Current commercial spacecraft attitude sensors range in cost from \$150,000 to greater than \$1,000,000 with quoted accuracies of a few hundredths to a few thousandths of a degree. Some of the larger, more expensive types of attitude sensors, such as star trackers which detect the positions of known star fields. Infrared (IR) horizon sensors, commonly used on Earth-orbiting satellites, monitor the position of the Earth's horizon by measuring the altitude gradient of infrared radiation in the atmosphere. Whereas current IR horizon sensors provide tracking accuracy of  $\sim 0.05$ - $0.1^\circ$  RSAS could easily resolve to  $0.01^\circ$ . The GSFC ultraviolet radiative transfer code predicts that the 355 nm limb radiance decreases by 15% per km at altitudes above 20 km<sup>2</sup>. By way of comparison, IR flux varies by only 2% per km along a vertical column of atmosphere, and can fluctuate with season and weather. The large UV gradient allows a more accurate measurement of the position of the horizon and thus spacecraft attitude than standard IR techniques. RSAS could thus provide up to an order of magnitude performance gain over current horizon sensors.

RSAS further demonstrates other applications of viewing the Earth's limb radiances in the ultraviolet. Limb remote sensing has the potential for measuring accurate, high altitude resolution profiles of ozone, aerosol, and possibly water vapor and temperature. The Limb Ozone Retrieval Experiment (LORE) and the Shuttle Ozone Limb Sounding Experiment (SOLSE) will employ this technique to measure high vertical resolution ozone profiles. This technique could be useful for future limb imaging instruments that require highly accurate knowledge of the viewing location for atmospheric modeling, and has already been proposed for the Atmospheric Pollution, Aerosol, and Chemistry Satellite (APACS).

In addition to testing the limb-scattering detection process, RSAS was also a technology demonstration platform for its components. For instance, the ultra-stable, narrow bandpass UV filter used by RSAS has become available only very recently and was flight-proven by RSAS. This 355 nm UV filter, whose coatings were deposited using "hardened" techniques<sup>1</sup> RSAS, provides the 10 nm bandpass range that RSAS requires. Additionally, RSAS data are used to validate recent modifications and improvements to the GSFC ultraviolet radiative transfer model that allow accurate prediction of the UV flux under such variations as changing solar zenith angle (SZA) and azimuth angle, and the non-uniform reflectivity of the Earth's surface<sup>2</sup>.

## 2.0 DESIGN

### 2.1 Requirements Overview

#### 2.1.1. RSAS Attitude Determination

The technique employed to deduce attitude makes use of the steep gradient in the Rayleigh scattering function for altitudes above 20 km. Viewed at a wavelength of 355 nm, where ozone absorption is negligible and above aerosol scattering, the limb radiance falls off at a rate of about 15% per kilometer. This gradient provides an easy to detect

---

<sup>a</sup> SSBUV, also developed at GSFC, consists of two Get Away Special (GAS) canisters. It measures atmospheric ozone concentrations by comparing direct solar ultraviolet radiation with radiation backscattered from the Earth's atmosphere. SSBUV compares the observations of several ozone measuring instruments aboard the National Oceanic and Atmospheric Administration NOAA-9, NOAA-11, and NOAA-14 satellites, the Russian Meteor-3/TOMS satellite and GSFC's Upper Atmosphere Research Satellite (UARS). SSBUV data are used to calibrate these instruments and ensure the most accurate readings possible for the detection of atmospheric ozone trends. RSAS was flown on one of the SSBUV canisters during STS-72.

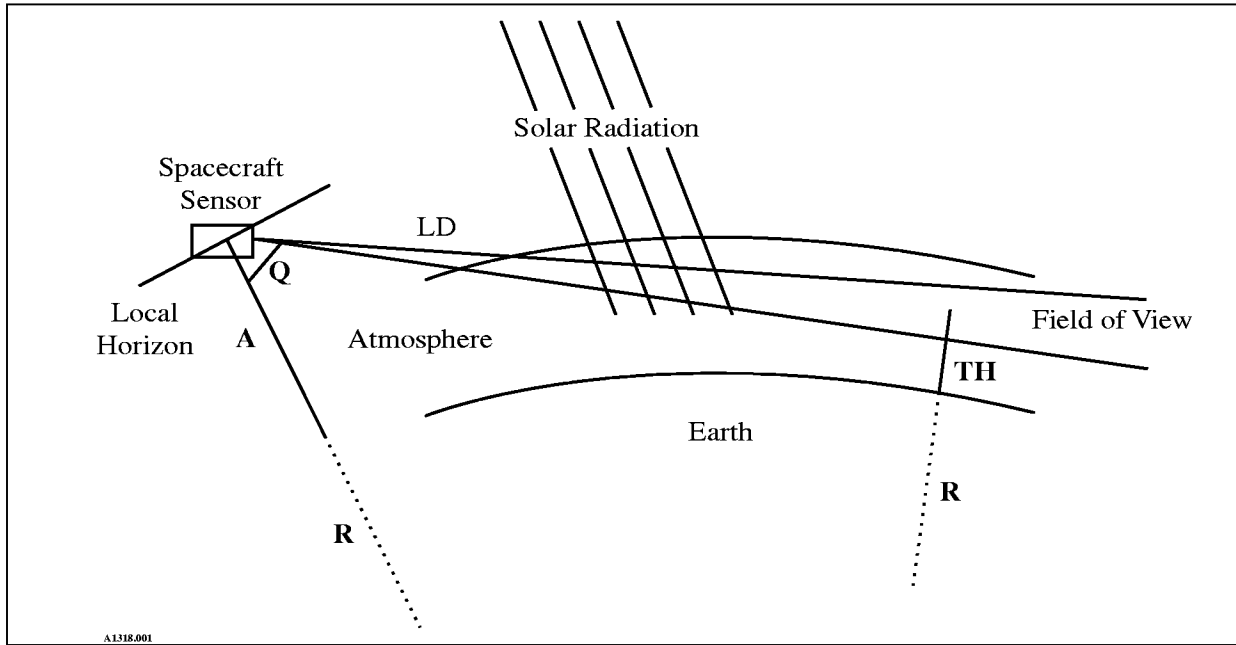


Figure 1. Limb viewing geometry.

signature, where changes in radiance at the instrument boresight location indicate changes in the tangent height (or a vertical altitude) of the scene in view. Once the change in tangent height is determined, the change in spacecraft pointing angle (and thus spacecraft attitude) can be calculated.

As shown in figure 1, the optical axis of RSAS was inclined at an angle  $(90^\circ - \Theta)$  from the local horizon in order to center its field of view (FOV) at the correct altitude on the limb. From this viewing geometry the attitude angle  $\Theta$  can be derived from

$$\sin \Theta = \frac{R + TH}{R + A}, \quad (1)$$

where R is the radius of the Earth, TH is the tangent height, LD is the line of sight distance to the limb, and A is the spacecraft altitude. For an Orbiter altitude of 306 km and the desired FOV centerline limb tangent height of 30 km, the limb distance was found to be 1899 km and  $\Theta$  was determined to be  $73.4^\circ$ .

### 2.1.2 Physical Description

An isometric diagram of Rayleigh-scattered solar radiation passing into RSAS is shown in figure 2. Incident radiation first passes through the filter, provided by Optical Corporation of America (OCA), where 355 nm radiation with a bandpass of 10 nm is allowed through the telescope lens. The UV light is then reflected by the transfer mirror onto the pixels of the detector array, where it induces a charge build-up on the photodiodes.

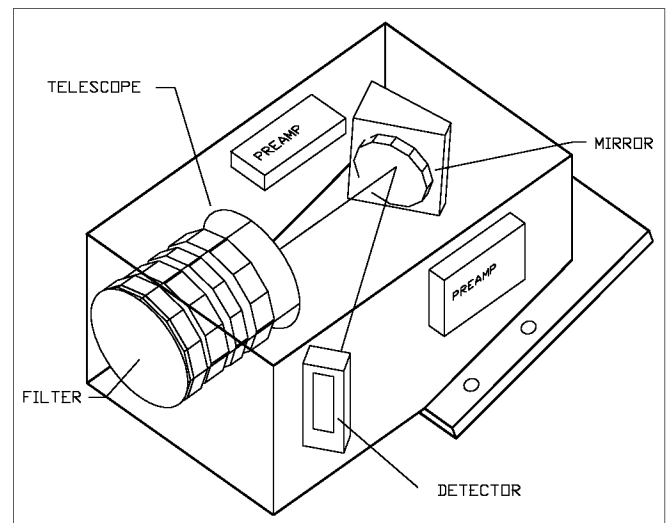


Figure 2. Optics module.

## 2.2 System Overview

The first of the system's two mechanical components, the optics module, includes the high quantum efficiency, solid-state, linear (512-pixel) photodiode detector array and preamplification electronics, a lens and filter arrangement, and a transfer mirror. The photodiode array elements are  $25\ \mu\text{m} \times 2.5\ \text{mm}$  in size and are spaced  $25\ \mu\text{m}$  center to center. The camera's focal length of 12 cm and full FOV of  $6^\circ$  correspond to a pixel FOV of  $\sim 0.01^\circ$ . From an altitude of 306 km, this provides a per pixel resolution of 0.35 km at the Earth's limb. The high stability, advanced interference filter provides an out-of-band to in-band response ratio on the order of  $10^{-7}$ . The optics module is about four inches long and two inches wide, and was designed to fit into a small volume (usually used by one of the SSBUV instrument's four IR horizon sensors) on the top deck of the SSBUV payload. The angle of elevation of the optical axis of RSAS from the SSBUV mounting plate is equal to the pointing angle  $\Theta$ . (See figure 1).

The second component of the RSAS system, the controller module, houses both the power subsystem and the digital control and avionics electronics, enables command and control of the RSAS system (including power ON/OFF and regulation of detector integration times), and was mounted just below the top deck of the SSBUV payload during STS-72. The entire RSAS system is pictured in figure 3.

## 2.3 Radiometric Characterization

The radiometric performance parameters for RSAS were determined in an analysis by Research and Support Instruments, Inc. (RSI). Using the GSFC ultraviolet radiative transfer code, the limb radiance for  $\lambda = 355\ \text{nm}$  was modeled as a function of altitude, SZA, and surface reflectivity. It was determined from the model that the maximum and minimum values for the bi-directional scattering distribution function (BDSF) of 355 nm UV flux at an altitude of 30 km were  $0.1\ \text{sr}^{-1}$  and  $0.02\ \text{sr}^{-1}$ , respectively. The minimum BDSF at 40 km was expected to be

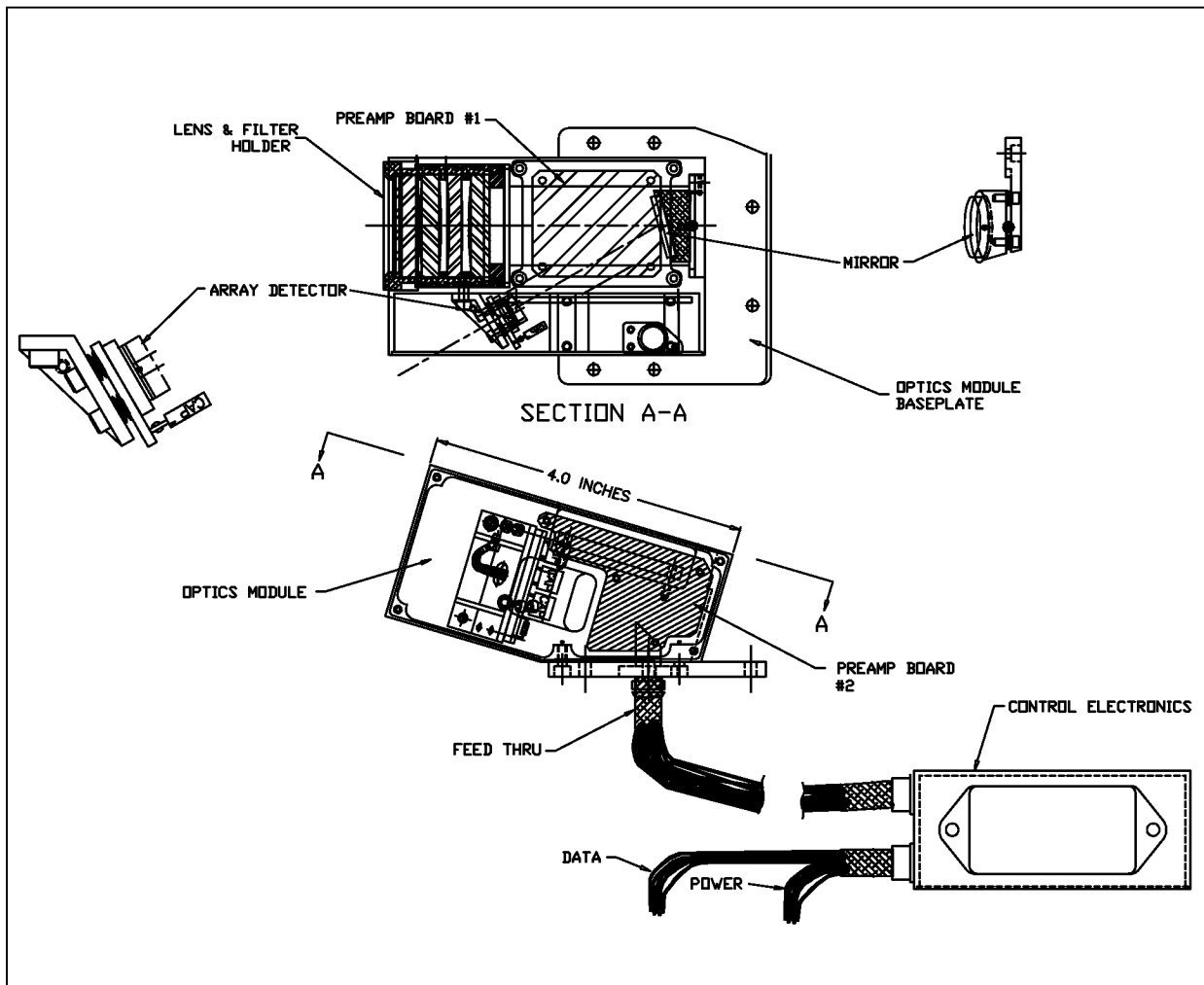


Figure 3. RSAS system diagram.

0.006 sr<sup>-1</sup>. The nominal flux density of solar radiation at 355 nm ( $E\{355\text{ nm}\}$ ) is a constant  $1.1 \times 10^{-4}$  W/(cm<sup>2</sup> nm). The limb radiance (L) at this wavelength and limb tangent height was then determined according to equation 2:

$$L\{355\text{ nm}, TH\} = BDSF\{355\text{ nm}, TH\} \times E\{355\text{ nm}\} \quad (2)$$

The values of L over the range of possible altitudes at constant E are given in Table 1.

**Table 1. Limb Radiance for Min/Max BSDF at Three Altitudes**

Limb Altitude	L{355 nm} (W/(cm <sup>2</sup> nm sr))	
	Minimum	Maximum
20 km	$1.0 \times 10^{-5}$	$2.0 \times 10^{-5}$
30 km	$3.3 \times 10^{-6}$	$1.1 \times 10^{-5}$
40 km	$6.7 \times 10^{-7}$	$2.0 \times 10^{-6}$

The theoretical signal per pixel (S/P) is given by equation 3:

$$S / P = (L)(\Delta\lambda)(\Omega_L)(A_{PIXEL})(T_L)(T_F)(R_\lambda), \quad (3)$$

where  $\Delta\lambda$  is the bandpass of the UV filter, and  $\Omega_L = 3.6 \times 10^{-2}$  sr is the solid angle subtended over the instrument's FOV. The value of  $A_{PIXEL}$ , the surface area of each of the 512 pixels in the linear array, is  $6.25 \times 10^{-4}$  cm<sup>2</sup>. The filter and lens transmittance,  $T_F$  and  $T_L$ , were determined experimentally by RSI to be 0.6 and 0.8, respectively. The photodiode pixel response  $R_\lambda$  at 355 nm is 0.1 A/W. These parameters yield an S/P of 97 pA at the maximum value for limb radiance L. Charge saturation, or "full well," for a Reticon SC linear array pixel is  $1 \times 10^{-11}$  C. Therefore, the integration time was calculated to be no longer than about 0.1 s. For a dark current (DC) of 0.2 pA, estimates for full well signal and amplifier noise were made. Signal-to-noise (S/N) for full well was calculated to be  $2.3 \times 10^4$  for the theoretical maximum signal at 30 km. For the theoretical minimum signal occurring at 40 km, predicted S/N dropped to  $1.4 \times 10^3$ .

The theoretical altitude resolution (TAR) shown below was calculated by dividing the line of sight distance to the limb (LD = 1899 km) by the focal length, and then multiplying by the height of one pixel ( $h_p = 25 \mu\text{m}$ ) as shown in equation 4:

$$TAR = \left( \frac{LD}{F} \right) h_p \quad (4)$$

According to the above relation, the TAR was found to be 0.39 km/pixel. RSAS's optical parameters, are summarized in Table 2.

**Table 2. Optical Characteristics**

Limb Distance (nominal)	LD = 1899 km
Focal Length	F = 12.0 cm
Lens Diameter	D = 3.5 cm
Focal Distance	F = 12 cm
Integration Time	T = 0.1 s
Signal per Pixel	S/P = 97 pA
Dark Current	DC = 0.2 pA
Filter Bandpass	$\Delta\lambda = 10$ nm
FOV Solid Angle	$\Omega_L = 3.6 \times 10^{-2}$ sr
Pixel Height	$h_p = 25 \mu\text{m}$
Pixel Width	$w_p = 2.5$ mm
Pixel Area	$A_{PIXEL} = 6.25 \times 10^{-4}$ cm <sup>2</sup>
Filter Transmittance	$T_F = 0.6$
Lens Transmittance	$T_L = 0.8$
355 nm Linear Diode Response	$R_\lambda = 0.1$ A/W
Theoretical Altitude Resolution	TAR = 0.35 km/pixel

## 2.4 Hardware Design

### 2.4.1 Mechanical Description

The RSAS system was designed to share the existing SSBUV mechanical platform, and to use SSBUV's power and data output systems. The mechanical and optical design was constrained by the space available on the top deck of the SSBUV canister. Mechanically, RSAS is comprised of two components: The optics and the controller modules. The optics module replaces one of the SSBUV payload's four horizon sensors on the top deck of the canister, as shown in figure 4.

The control module is situated just beneath the top deck of the SSBUV canister. It is connected to the SSBUV power bus, and also to the RSAS optics module via a hole in the canister and the mounting plate. The optics module and controller module weigh 1.43 lb. and 1.10 lb., respectively, and are made from Aluminum 6061-T6. The optics module is coated with silver Teflon and the controller module has an irridite finish. Together, both units consume a total system power of 4.2 W.

### 2.4.2 Electrical Description

#### 2.4.2.1 Signal Processing

The incoming radiation, passing through the filter and telescope, strikes the 512-pixel linear photodiode array, where a charge proportional to the incident light intensity is generated on each pixel. The current induced by the charge buildup is amplified by the RSAS preamplifier circuitry, conditioned, and transferred to the controller module as a voltage.

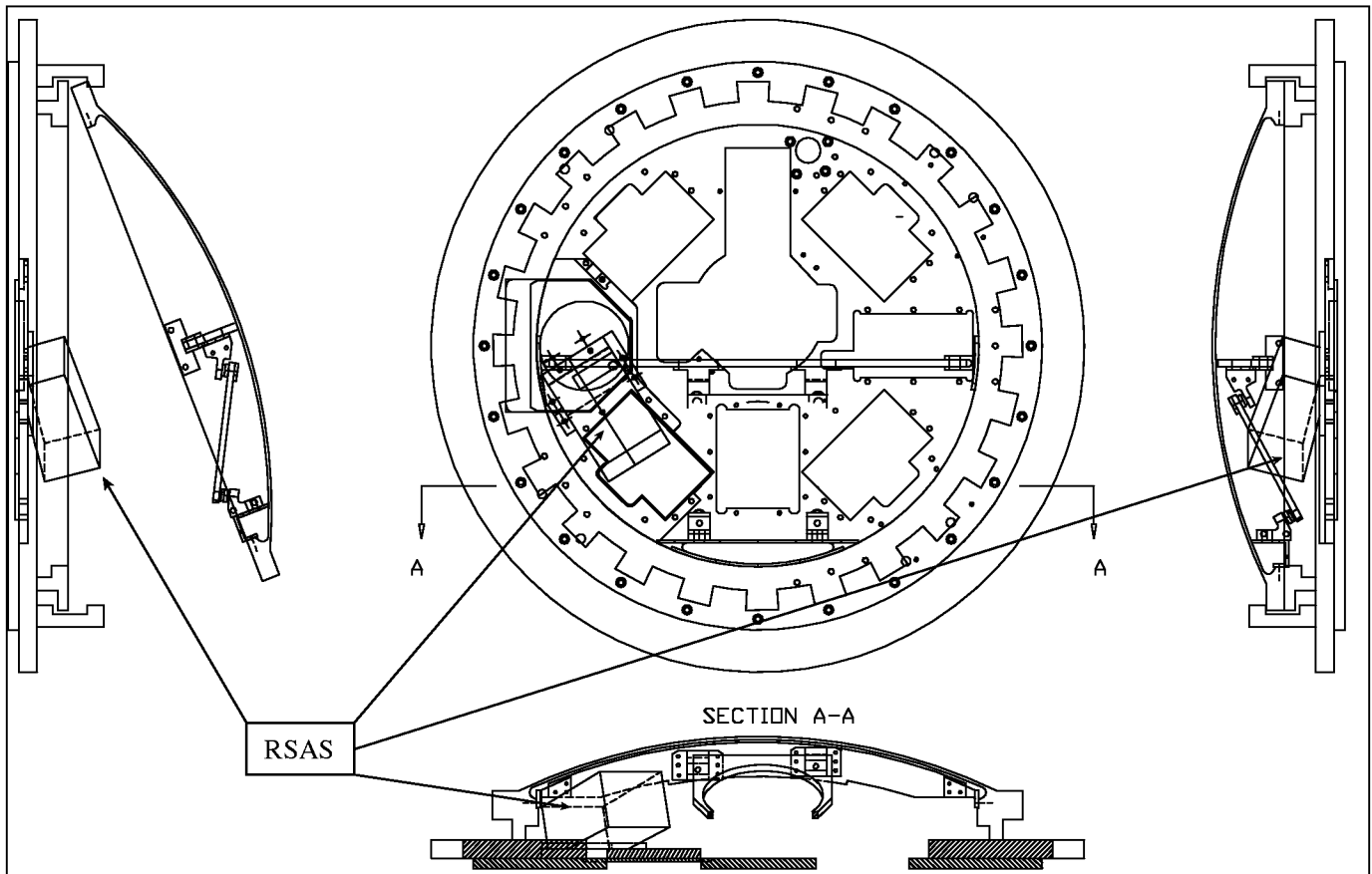


**Figure 4. RSAS mounted in SSBUV GAS canister.**

The analog diode charge output voltage is converted to a digital signal using a 14-bit analog-to-digital (A/D) converter. The controller module circuitry was also responsible for configuring the RSAS system for data acquisition by translating RSAS commands. Ancillary electronics were used to control, buffer, and transfer the flight data through the controller to the SSBUV avionics electronics. Figure 5 illustrates the electronic components of RSAS.

#### **2.4.2.2 Optics Module Electronics**

There are three main electrical components in the optics module. The Reticon EG&G (RL0512SCQ-011) photodiode array was chosen for its radiometric performance, small size, and serial output. This array and the ancillary discrete components reside on one printed circuit board (PCB). The dual preamplifier design is based on the first stage differential recharge mode video amplifier from the Reticon EG&G Evaluation Circuit (RC1032LNN-011). The preamplifier consists of two PCB mounted are the optics module as shown in figure 2. This design was necessary to make the best use of the small space available. The final component of the optics module is the set of command line drivers.

The active and dummy (dark current) video outputs of the sensor array are fed to a preamplifier PCB where they are differentially amplified by the first amplifier stage for noise reduction. The output is essentially a train of voltage pulses corresponding to the charges detected on each photodiode as they are read out in sequence. The second amplifier stage subtracts a positive DC voltage level video line bias from the signal, while a third stage integrates the video signal. The second preamplifier board generates the necessary voltage references used by the first preamplifier PCB, as well as conditioning other necessary sensor chip control signals. The video output of this preamplifier is then sent to the controller module.

#### **2.4.2.3 Controller Module Electronics**

The major components of the controller module are the A/D converter, the first-in first-out (FIFO) data buffer, three field programmable gate arrays (FPGA) for controller logic and a local clock, an additional preamplifier stage, a power supply module (a DC/DC converter that converts Orbiter-supplied power) and an EMI filter. The FPGAs, manufactured by Actel, Inc. (A101B) contain 1200 gates. These FPGAs not only generates all clocks needed by the photo-

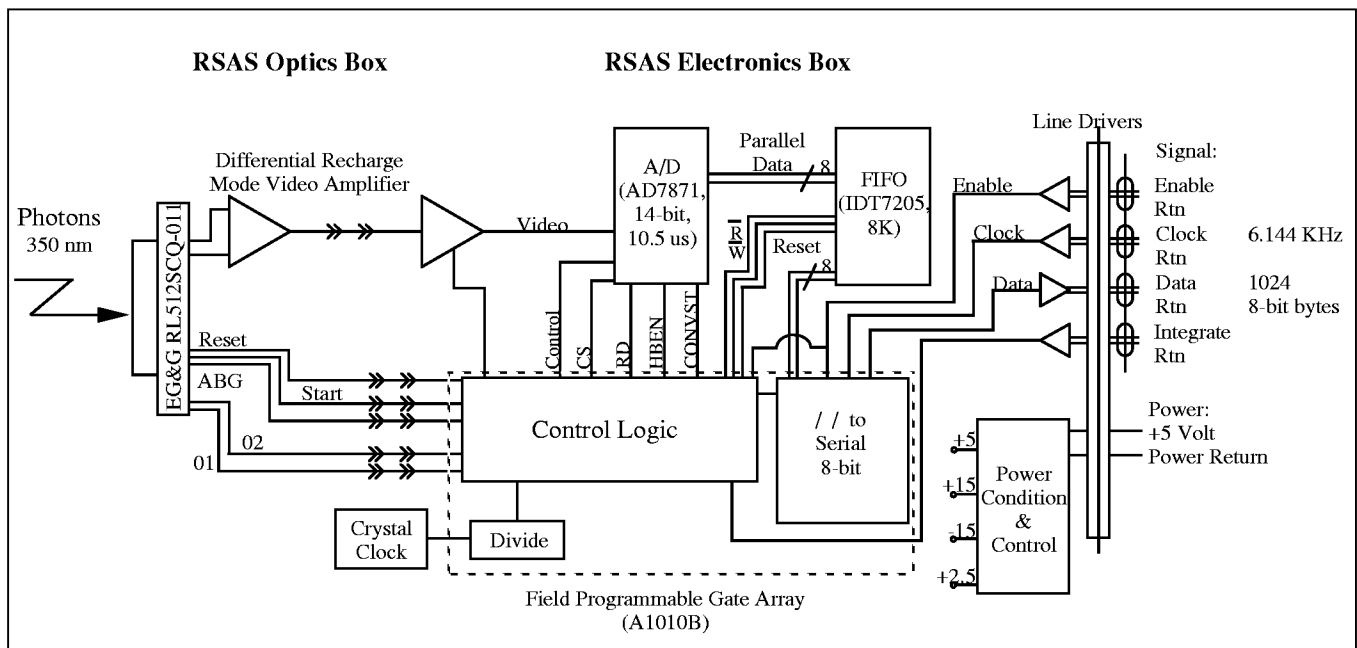


Figure 5. RSAS electrical block diagram.

diode array, the A/D converter, and the FIFO, but also have a parallel to serial converter for use in data transfer. The A/D converter is a 14-bit CS5014 unit whose output is in two 8-bit words. The IDT7205 FIFO has 8 kilobytes of storage.

The preamplifier stages are derived from the EG&G Evaluation Circuit, but do not include a sample-and-hold stage. The 5 V quiet DC power supply module actually is an externally mounted, triple output DC/DC converter that transforms the 28 V unregulated DC power coming from the Orbiter via the removed nadir sensor's connector. An EMI filter provides well-conditioned power to both the controller module and the optics module at the appropriate voltage levels.

## 2.5 Software Design

The software written for RSAS serves several independent functions. Certain existing programs were modified to accommodate RSAS on the SSBUV payload. Initially, the original SSBUV avionics software needed to be modified to allow for control and handling of the incoming RSAS data stream. Software was written in FORTH (the operating system of the SSBUV computer) to utilize SSBUV ground support equipment for testing and evaluating the RSAS system at several stages of system development. Because of the fast-paced development schedule, this software was needed especially to identify system problems so that they could be corrected as soon as possible. Since the development of both the optics module and the controller module occurred in parallel, a method of testing the sensor module was needed early in the development of the system hardware. As the hardware development progressed, several

software and test harness packages were fabricated to provide quality assurance testing at each stage of development. Detector integration time was under software control and commandable via the ground support equipment (GSE).

### 2.5.1 RSAS Component Drivers

The controller module FPGA logic was programmed using the VHDL design language to implement RSAS system control features. Once programmed, these FPGAs provided a method of synthesizing logic that resulted in a significant savings in the number and size of the discrete electronic components that would have otherwise been necessary to implement the control features required by the RSAS system specifications. The end result was an electronics control capability that easily fit the volumetric, weight, and power restrictions required by the placement of RSAS on the SSBUV platform.

### 2.5.2 Ground Support Equipment Software

Changes to the SSBUV avionics code (again in the FORTH language) had to be made in order to accommodate command and control of the RSAS avionics system. The SSBUV avionics system was well-established and flight-proven. Since it was the vehicle for sending commands to and receiving telemetry from the RSAS system, great care had to be taken to provide software capability for all the RSAS system functions without affecting any of the flight-critical SSBUV software or exceeding the confines of the SSBUV avionics. Specifically, RSAS GSE software for the STS-72 flight consisted of a 80386 Ur/ FORTH program that was capable of sending the RSAS integration time,

flushing the RSAS data stream, reading and storing blocks of data, and displaying the data as either a graph or a table.

Other ground system segment software was modified not only to enable the sending of RSAS system commands, but also to allow receipt and display of the RSAS telemetry and science data. These programs were written in Turbo Pascal and ran on PC-based platforms. During the Shuttle flight, several multipurpose commands were available using SSBUV workstations to control the RSAS from the ground. These commands used a single parameter which allowed either power and response control (integration time was adjustable within the range 0.052 s–15 s), depending on the parameter entered.

### **2.5.3 RSAS Data Processing**

The RSAS data was interleaved into the SSBUV data stream without affecting it, as only unused SSBUV spare data words in the SSBUV telemetry stream were replaced with RSAS data. Each time a snapshot of the horizon was taken (every 80 seconds), RSAS raw data was organized into a single scan of size 1035 words (2070 bytes). This scan included 1,024 words—512 words for background and 512 words for 355 nm light intensity data on each pixel in the 512 pixel array. The remaining words were used either to record the integration time, the ambient temperature, or as buffer data bytes. Programs written in C++ and the Interactive Data Language (IDL) were used to extract the data from the SSBUV telemetry and convert pixel counts to calibrated engineering units.

## **2.6 Testing and Calibration**

### **2.6.1 Optical Calibration**

#### **2.6.1.1 Pre-Flight Optical Axis Alignment**

The optical axis of RSAS was aligned using a Davidson D 275 autocollimator optical alignment telescope, and an Oriel slit assembly. In order to isolate outside effects such as scattered light and optical cross-talk, the predicted signal distribution over a minimum number of pixels was compared with the actual measurement. The lens was then adjusted so that a minimum number of pixels were illuminated at an autocollimator beam incidence angle of 0°. With the RSAS optics module mounted on a goniometric fixture, the number of photodiode pixels illuminated was measured as a function of autocollimator beam incidence angle in steps of 0.1° over the 6.0° FOV of the instrument. Also, the azimuthal response of the detector was measured as a function of elevation angle at each whole degree from -3.0° to 3.0°. After these measurements, fine adjustments of the lens barrel were made to obtain the peak response. The slit center was thus aligned with respect to the mechanical axis of the lens assembly.

The true optical focus was determined in the visible by using the autocollimator alignment telescope, and was measured at 12.0 cm. With the autocollimator focused on infinity, RSAS' lens was moved until the image on the linear array was focused onto the image plane of the autocollimator. By finding the position of minimum image width of an illuminated slit, RSAS' focal length was finely adjusted. To adjust the system for 355 nm radiation the instrument was illuminated with a precision slit with a width of 0.25 mm at a distance of 2.58 m. The focal length found using this method was 12.58 cm, which verified the theoretical calculation. Finally, the infinity and vacuum values for the focal length were calculated for the final lens positioning.

The machining tolerance of the elevation of the RSAS housing (1 arc minute) was verified with the an optical flat and the autocollimator alignment telescope. Resolution across the full FOV of the instrument was verified by mounting RSAS on a rotary table and measuring the image width of the illuminated slit as a function of scan angle. This was done along two orthogonal axes, one with the slit image parallel, and one with the image perpendicular to the 2.5 mm pixel length. Before flight, the RSAS optics module was tested for angle alignment and finely tuned.

#### **2.6.1.2 Pre-Flight and Post-Flight Radiometric Calibration**

RSAS was calibrated for image quality and absolute sensitivity both prior to and after the Space Shuttle flight. The filter bandpass and center wavelength were also measured pre-flight and post-flight. Prior to flight, the lens barrel was repositioned for imaging the limb at a range of 1900 km. Out-of-band filter transmittance was characterized using RSI's double monochromator system, and was found to be less than 10<sup>-6</sup>.

The image quality and FOV mapping consisted of scanning the instrument in elevation and azimuth while viewing a slit and recording the resultant image with the photo diode array. The FOV measurements agreed with the calculated values of 6.1° x 1.2° with an out-of-field response less than 10<sup>-6</sup>. The full width at half maximum (FWHM) of the slit image ranged from 25µm at center to 70µm at ± 2.8°. The post-flight measurement of these quantities showed little or no change.

The absolute calibration was performed using a NASA 20" internally-illuminated, large-aperture spherical integrator. The calibration technique consists of illuminating the instrument with a uniform, large-area source of known radiance. The radiometric stability of RSAS' optical system was demonstrated by measuring its response to the spectral radiance of the aperture in 10 minute intervals over a 2 hour period. The device's polarization sensitivity was also measured using a 2" diameter UV polarizer, and

intensity losses due to polarization were recorded in 5° increments of polarizer rotation angle. Differences in sphere radiance over the 3.8° FOV were accounted for by varying RSAS' distance from the integrator. The calculated infinity and vacuum focal lengths for RSAS were also verified. The exact calibration procedures are described in more detail elsewhere<sup>3,4,5</sup>.

The results of the post-flight calibration showed a drop in instrument sensitivity of about 3%. This has been traced to a shift in the center bandpass of the interference filter by about 0.2 nm, as shown in Figure 6, below. This shift to shorter wavelengths reduces the apparent radiance of the source. The reason for the change in the filter behavior is not known and is currently being investigated. This shift in band pass has no effect on the performance of RSAS with respect to attitude sensing.

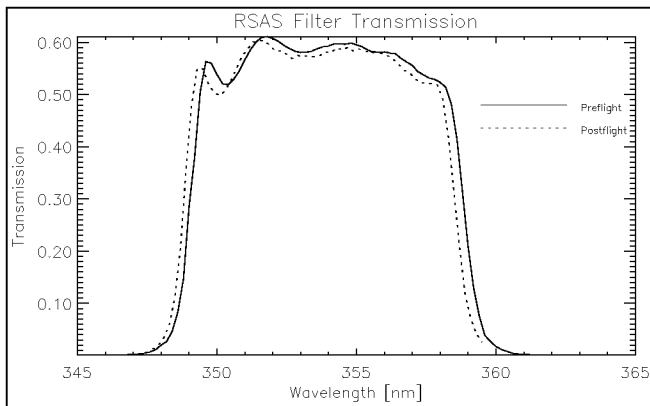


**Figure 6. Variations in pre-flight to post-flight filter transmittance.**

## 2.6.2 Structural/Mechanical Analysis and Testing

### 2.6.2.1 Vibration Test

The RSAS system underwent a vibration test to verify stability, structural soundness, and workmanship. This test provided no evidence of potentially dangerous resonant frequencies for the system. All loads experienced by the system during the vibration did not place undue stress on any of the components. It was determined that RSAS was not in danger of being damaged by any vibration that could have occurred during the launch of STS-72.

### 2.6.2.2 Stress and Fracture Analysis

The anticipated load levels used in the stress analysis of RSAS were taken from Get Away Special (GAS) documents detailing load levels undergone by the SSBUV instrument on previous STS flights. These levels are  $\pm 11$  g's in the Orbiter's x, y, and z axes. The margins of safety were determined using factors of safety of 2.0 and

2.6 for material yield and ultimate strength, respectively. The smallest margin of safety was 9.7 for the fail-safe analysis of the fasteners holding the mounting plate to the housing. The margins of safety are shown in Table 3.

**Table 3. Expected Stress Levels**

Description	Bolts	Margin of Safety
Mounting Plate to SSBUV Plate	#6-32	11.8
Mounting Plate to Housing	#4-40	9.7
Optics Barrel Axial Stress	—	275
Optics Barrel Hoop Stress	—	17.3
Controller Box	#6-32	16.2

## 2.6.3 Thermal Environment Analysis

Preliminary thermal environment computational predictions were performed by Swales & Associates, Inc. Using solar incidence angles based on data from SSBUV's previous mission (STS-66), it was concluded that during its use the temperature of the uncoated (white) RSAS optics module would fluctuate by no more than  $\pm 3^\circ$  about a mean value of  $17^\circ\text{C}$ . It was predicted that RSAS' optics module would always be slightly hotter than the top deck of the SSBUV canister, whose median temperature would be approximately  $15^\circ\text{C}$ .

Later analyses, based on modeled solar and Earth reflectance incidence angles for STS-72, predicted that the temperature of the optics module would vary between  $17^\circ\text{C}$  and  $23^\circ\text{C}$ , slightly higher than the original model had estimated. In either case, however, the temperatures were not expected to leave the operational range of  $0^\circ\text{C}$  to  $40^\circ\text{C}$  at any time during the mission. Although both analyses were performed under the assumption that the RSAS optics module would fly uncoated, it was covered with silver Teflon before STS-72. The silver Teflon tape was applied to act as an insulator, to reduce heat transfer to and from RSAS, and to keep the temperature variations down.

## 3.0 PERFORMANCE

While other instruments have used the Rayleigh scattered limb signal to deduce viewing altitude<sup>6,7</sup>, RSAS was designed solely to test this concept and was flown alongside traditional infrared horizon detectors on the Space Shuttle. Along with the Shuttle attitude system, which consists of star trackers and inertial devices, ground-based radar altitude

measurements provided an accurate ( $0.05^\circ$ ) baseline for evaluating the performance of RSAS. In the following sections, both the algorithm used to convert limb radiance data to pointing information and results from the first flight of this instrument are presented.

### 3.1 STS-72 Payload Configuration

During the test flight, the SSBUV GAS canister was situated on the starboard side of the Orbiter, as illustrated in figure 7, below. RSAS was mounted on the top deck of the SSBUV canister, and its lens was inclined at the pointing angle of approximately  $16.5^\circ$  with respect to the local horizon. The azimuth pointing orientation was  $32.1^\circ$  with respect to the Orbiter's y-axis.

RSAS collected data when the Orbiter's payload bay and the SSBUV GAS canister lid were open. Also, since the RSAS optics module was fixed in orientation with respect to the

Orbiter, a constant bay-to-Earth attitude had to be maintained to obtain useful data. All attempts were made to ensure that RSAS had a clear FOV.

### 3.2 Analysis Methodology

The limb radiance measured by RSAS is a function of SZA and azimuth angles (lighting conditions), altitude and pointing, and the reflectivity of the Earth and atmosphere below the viewing altitude. To simplify the calculation of altitude and pointing changes, the lighting conditions and reflectivity dependence can be virtually eliminated using a ratio technique. This technique makes use of the observation that the shape of the limb radiance signal is nearly independent of these varying factors. The left chart in figure 8 shows the limb radiance signal as a function of altitude. To the right, the ratio of the nominal boresight signal at an altitude of 30 km to the same signal at 20 km is

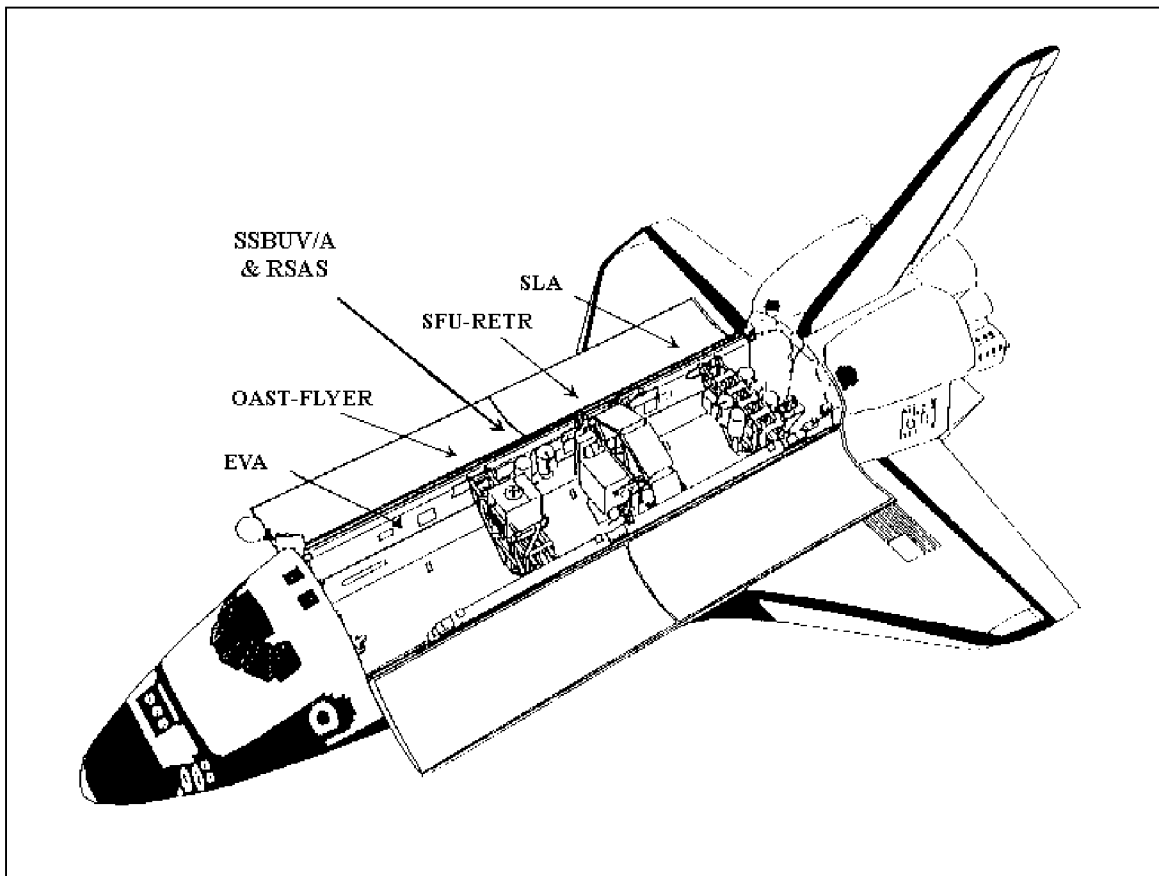
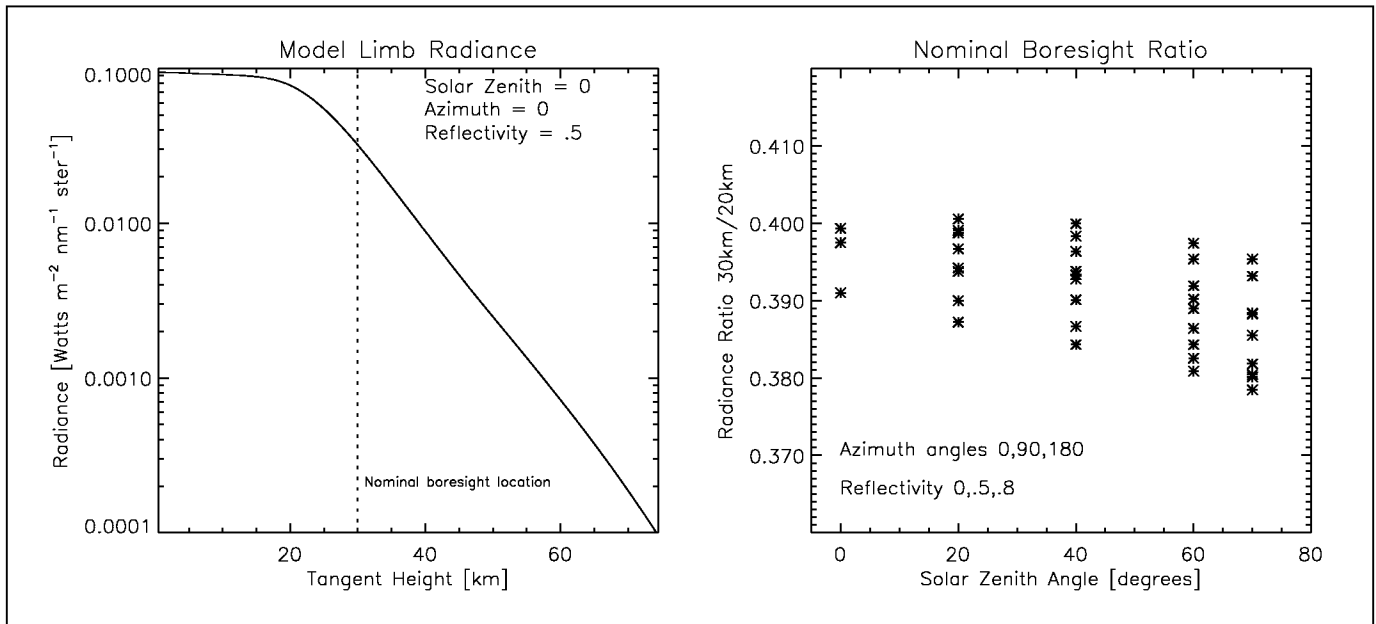


Figure 7. STS-72 payload orientation.



**Figure 8. Model radiance and radiance ratio under various lighting conditions.**

shown as a function of SZA for a wide range of lighting conditions and surface reflectivity values. The chart on the right shows that this ratio changes very little over these conditions, even though the radiance may change substantially.

The variations shown in the figure do imply potential modeling errors on the order of  $0.01^\circ$ . Additionally, errors on the order of  $0.05^\circ$  can exist for SZAs greater than  $80^\circ$ . Therefore, the data analysis is restricted to SZAs less than  $80^\circ$ . During the mission, RSAS images were taken during 46 orbits at a rate of one every 80 seconds. Because the limb filled roughly half the RSAS FOV, pixels pointed above the atmosphere could be used to correct for dark current and stray light.

### 3.3 Results

The GSFC ultraviolet radiative transfer code was used to model the expected 355 nm radiance during various periods of the STS-72 flight, and a theoretical altitude gradient for UV radiance was generated. To best compare the actual data with the predicted data, a series of normalized radiances as a function of tangent height (TH) was created. This series is shown in figure 9, along with the same ratio calculated from an RSAS image during the actual Shuttle flight. The similarity in the shape of both curves can easily be discerned. Although each set of data has been normalized, the variation in the measured UV flux with altitude matches the model very closely. The limb ratio measured at the boresight pixel was then converted to a tangent height by comparing the normalized radiance with the model calculations using equation 1.

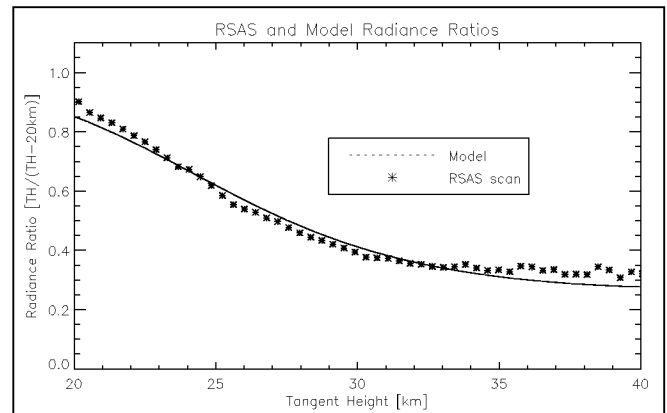


**Figure 9. Normalized radiance vs. altitude.**

The RSAS calculated pointing changes were then compared to the shuttle measured values using the post-flight attitude and trajectory history (PATH) data<sup>8</sup>. The PATH data has a quoted accuracy of 1 km in altitude and  $0.05^\circ$ /axis in attitude per standard deviation. Figure 10 compares the elevation angle of the RSAS boresight with respect to the Shuttle's x-y plane to the Shuttle's known attitude measurements, using both the RSAS limb data and the PATH product during one daylight pass. From figure 11, it is evident that RSAS indicates a consistent offset with respect to the PATH data. Figure 11 shows the difference between the two measurements over a series of orbits. Also plotted in figure 11 is the SSBUV Sun sensor measurement of the same offset during a subsequent orbit. It can be seen that the Sun sensor agrees well with the RSAS measured offset. The measured elevation difference between the SSBUV top deck and the shuttle x-y plane was  $0.08^\circ \pm 0.05^\circ$ .

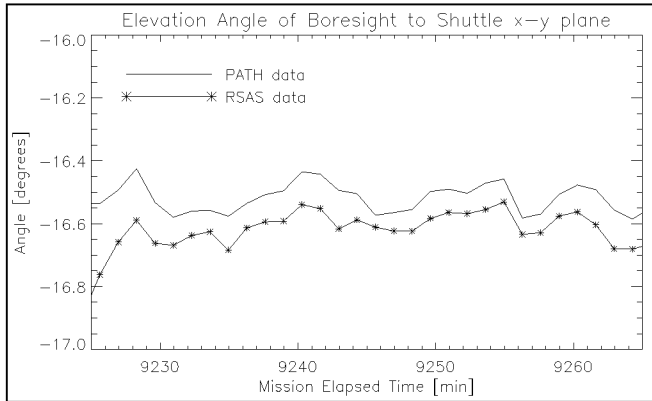


**Figure 10. Elevation angle measured by RSAS and PATH.**

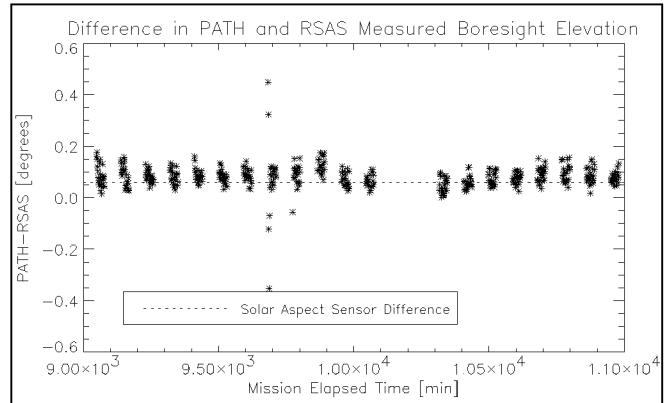


**Figure 11. Differences in elevation angle as measured by RSAS, PATH, and SSBUV Sun sensor.**

## 4.0 SUMMARY

The Rayleigh Scattering Attitude Sensor was designed, built, tested, and flown on the Space Shuttle by personnel at the NASA GSFC. Motivation for the design stemmed from the possibility of developing a very accurate spacecraft horizon sensor at low cost, while at the same time providing a test bed for new technologies and improvements to current radiative transfer models. Several aspects of the overall design have been documented, including initial requirements, hardware specifications, and explanations of software support systems. Additionally, system testing procedures and results have been explained, and pre-flight and post-flight calibration differences have been summarized. Finally, the test-flight configuration, data retrieval procedures, and initial performance analysis have been presented.

RSAS has succeeded in proving the concept of using a UV limb detector for spacecraft attitude determination purposes. This novel attitude sensor that detects Rayleigh-scattered solar radiation has successfully completed its tests on the Space Shuttle Endeavor during the STS-72 flight. RSAS performed as good or better than expected, by producing measurements of its boresight pointing angle accurate to at least  $0.05^\circ$ . In principle, this accuracy can be improved by carefully considering optical system aberrations, better modeling the varying factors that alter the nominal UV radiance profile, and improving the component precision of the RSAS system.

## REFERENCES

- <sup>1</sup> M. Scoby and P. Stupik. "Stable ultra-narrow band pass filter," Presented at SPIE Annual Conference, July 1994.
- <sup>2</sup> B. Herman, D. E. Flittner, R. D. McPeters, and P. K. Bhartia, "Monitoring atmospheric ozone from space limb scatter measurements," *Proc. SPIE* Vol. 2583, p. 88, September 1995.
- <sup>3</sup> J. H. Walker, C. L. Cromer, and J. T. McLean, "A Technique for Improving the Calibration of Large-Area Sphere Sources," *Proc. SPIE*, Vol. 1493, pp. 224-230, April 1991.
- <sup>4</sup> D. F. Heath, W. Zhongying, W. K. Fowler, and V. W. Nelson, "Comparison of spectral radiance calibrations of SBUV-2 satellite ozone monitoring instruments using integrating sphere and flat-plate diffuser techniques", *Metrologia*, Vol. 30, pp. 259-264, October 1993.
- <sup>5</sup> S. J. Janz, E. Hilsenrath, J. Butler, D. F. Heath, and R. P. Cebula, "Uncertainties in radiance calibrations of backscatter ultraviolet (BUV) instruments," *Metrologia*, Vol. 32, pp. 637-641, May 1996.
- <sup>6</sup> H. J. Wang, D. M. Cunnold, and X. Bao, "A critical analysis of stratospheric aerosol and gas experiment ozone trends," *J. Geophys. Res.*, Vol. 101, pp. 12,495-12,514, May 1996.
- <sup>7</sup> D. W. Rusch, G. H. Mount, C. A. Barth, R. J. Thomas, and M. T. Callan, "Solar mesosphere explorer ultraviolet spectrometer: measurements of ozone in the 1.0-0.1 mbar region," *J. Geophys. Res.*, Vol. 89, pp. 11,677-11,687, December 1984.
- <sup>8</sup> A. S. King, "Final report for the STS-72 PATH product," *Johnson Space Flight Center Tech. Rep. 660-NAV-720-96-025*, April 1996.

# REPORT DOCUMENTATION PAGE

*Form Approved*  
OMB No. 0704-0188

Public reporting burden for this collection of information is estimated to average 1 hour per response, including the time for reviewing instructions, searching existing data sources, gathering and maintaining the data needed, and completing and reviewing the collection of information. Send comments regarding this burden estimate or any other aspect of this collection of information, including suggestions for reducing this burden, to Washington Headquarters Services, Directorate for Information Operations and Reports, 1215 Jefferson Davis Highway, Suite 1204, Arlington, VA 22202-4302, and to the Office of Management and Budget, Paperwork Reduction Project (0704-0188), Washington, DC 20503.

<b>1. AGENCY USE ONLY</b> ( <i>Leave blank</i> )		<b>2. REPORT DATE</b> September 1997	<b>3. REPORT TYPE AND DATES COVERED</b> Technical Memorandum	
<b>4. TITLE AND SUBTITLE</b>  Design, Development, and Test-Flight of the Rayleigh Scattering Attitude Sensor			<b>5. FUNDING NUMBERS</b>  NAS5 - 31729 NAS5 - 31755 (Code 916)	
<b>6. AUTHOR(S)</b>  E. Hilsenrath, Anderson, E. C., D. Flittner, D. Heath, S. Janz, J. Medeiros, J. Cerullo, C. Thorpe, T. Riley				
<b>7. PERFORMING ORGANIZATION NAME(S) AND ADDRESS (ES)</b> Laboratory for Atmospheres Goddard Space Flight Center Greenbelt, Maryland 20771			<b>8. PERFORMING ORGANIZATION REPORT NUMBER</b>  97B00044	
<b>9. SPONSORING / MONITORING AGENCY NAME(S) AND ADDRESS (ES)</b>  National Aeronautics and Space Administration Washington, DC 20546-0001			<b>10. SPONSORING / MONITORING AGENCY REPORT NUMBER</b>  TM-104644	
<b>11. SUPPLEMENTARY NOTES</b> E. C. Anderson, New Millennium Astronautics, Charlottesville, Virginia; D. Flittner, University of Arizona, Tucson, Arizona; D. Heath, Research Support Instruments, Boulder, Colorado; S. Janz, J. Medeiros, & J. Cerullo, The Aerospace Engineering Group of IDEA, Inc., Beltsville, Maryland				
<b>12a. DISTRIBUTION / AVAILABILITY STATEMENT</b>  Unclassified - Unlimited Subject Category: 19 Report available from the NASA Center for AeroSpace Information, 800 Elkridge Landing Road, Linthicum Heights, MD 21090; (301) 621-0390.			<b>12b. DISTRIBUTION CODE</b>	
<b>13. ABSTRACT</b> ( <i>Maximum 200 words</i> ) The Rayleigh Scattering Attitude Sensor (RSAS), a proof-of-concept device, was designed, developed, and tested, at the NASA Goddard Space Flight Center. The prototype instrument was flown aboard the Space Shuttle Endeavor (STS-72) in January 1996. RSAS uses a 512 element linear photodiode array and an interference filter to measure incident solar radiation that is Rayleigh-scattered from the Earth's limb at a wavelength of 355 nm. System requirements and a system overview are presented. Design and development of mechanical, electrical, and optical sub-systems of RSAS are also documented, including the software interface structure and ground support equipment (GSE). Pre-flight and post-flight testing procedures, calibration and optical characterization results are discussed. Limb scattering radiances observed by RSAS during the test flight show good agreement with predictions by the GSFC ultraviolet radiative transfer model. The attitude determination algorithm applied to the limb scattered signal is presented. The attitude measured by RSAS is shown to be in excellent agreement with concurrent Shuttle pointing data ( $\pm 0.05^\circ$ ). These data indicate that RSAS type instruments could yield significantly better performance ( $\sim 0.01^\circ$ resolution) than state-of-the-art horizon sensors ( $\sim 0.1^\circ$ resolution), at a considerably lower cost. Attitude Sensing, Ultraviolet, Rayleigh Scattering, Limb Scattering, Optics, Solar Radiation.				
<b>14. SUBJECT TERMS</b> Attitude Sensing, Ultraviolet, Rayleigh Scattering, Limb Scattering, Optics, Solar Radiation			<b>15. NUMBER OF PAGES</b> 18	
			<b>16. PRICE CODE</b>	
<b>17. SECURITY CLASSIFICATION OF REPORT</b> Unclassified	<b>18. SECURITY CLASSIFICATION OF THIS PAGE</b> Unclassified	<b>19. SECURITY CLASSIFICATION OF ABSTRACT</b> Unclassified	<b>20. LIMITATION OF ABSTRACT</b> UL	